Biochemistry

 Volume 41, Number 36 September 10, 2002

Current Topics

Comparative Models for Human Apolipoprotein A-I Bound to Lipid in Discoidal High-Density Lipoprotein Particles†

Anthony E. Klon,‡ Jere P. Segrest,‡,§ and Stephen C. Harvey*,‡

Department of Biochemistry and Molecular Genetics and Department of Medicine, University of Alabama at Birmingham, Birmingham, Alabama 35294-0005

Received April 26, 2002

ABSTRACT: We have constructed a series of models for apolipoprotein A-I (apo A-I) bound to discoidal high-density lipoprotein (HDL) particles, based upon the molecular belt model [Segrest, J. P., et al. (1999) *J. Biol. Chem. 274*, 31755−31758] and helical hairpin models [Rogers, D. P., et al. (1998) *Biochemistry 37*, 11714−11725], and compared these with picket fence models [Phillips, J. C., et al. (1997) *Biophys. J. 73*, 2337−2346]. Molecular belt models for discoidal HDL particles with differing diameters are presented, illustrating that the belt model can explain the discrete changes in HDL particle size observed experimentally. Hairpin models are discussed for the binding of apo A-I to discoidal HDL particles with diameters identical to those for the molecular belt model. Two models are presented for the binding of three monomers of apo A-I to a 150 Å diameter discoidal HDL particle. In one model, two monomers of apo A-I bind to the exterior of the HDL particle in an antiparallel belt, with a third monomer of apo A-I bound to the disk in a hairpin conformation. In the second model, all three monomers of apo A-I are bound to the discoidal HDL particle in a hairpin conformation. Previously published experimental data for each model are reviewed, with FRET favoring either the belt or hairpin models over the picket fence models for HDL particles with diameters of 105 Å. Naturally occurring mutations appear to favor the belt model for the 105 Å particles, while the 150 Å HDL particles favor the presence of at least one hairpin.

Apolipoprotein A-I (apo A-I)[1] is the major protein component of both nascent (discoidal) and circulating (spherical) high-density lipoprotein (HDL) particles. Elevated levels of HDL particles in the bloodstream have been shown to correlate with a reduced risk of atherosclerosis, the leading cause of coronary artery disease (*1*−*3*). Apo A-I has been shown to be responsible for a number of the antiatherogenic capabilities of HDL, including the activation of lecithin: cholesterol acyltransferase (LCAT) and the promotion of cellular efflux (*4*). As a result, the structure of apo A-I in HDL particles has been the subject of intense study.

Apo A-I is a 243-residue polypeptide which is divided into a 43-residue globular amino-terminal domain encoded by exon 3 of the apo A-I gene and a 200-residue lipid-binding domain encoded by exon 4 of the apo A-I gene at the carboxy terminus (*5*). The secondary structure of the lipid-binding

† This work was supported by a grant from the NIH to J.P.S. (PO1 HL 34343).

* To whom correspondence should be addressed. Telephone: (205) 934-5028. Fax: (205) 975-2547. E-mail: harvey@uab.edu.

‡ Department of Biochemistry and Molecular Genetics.

§ Department of Medicine.

[1] Abbreviations: apo A-I, apolipoprotein A-I; DMPC, dimyristoylphosphatidylcholine; FTIR, Fourier transform infrared; FRET, fluorescence resonance energy transfer; HDL, high-density lipoprotein; LCAT, lecithin:cholesterol acyltransferase; POPC, palmitoyloleoylphosphatidylcholine; rHDL, reconstituted high-density lipoprotein.

10.1021/bi020315m CCC: $22.00
Published on Web 08/16/2002

domain is dominated by 10 helical repeats that have been classified as amphipathic α-helices. Eight of these repeats are 22 residues in length, while two repeats are 11 residues in length, with most of these amphipathic α-helical repeats punctuated by a proline residue at the beginning of the repeat (*6*, *7*).

This review will consider the structure of apo A-I bound to discoidal HDL particles. The models for the binding of apo A-I to discoidal HDL particles presented to date fall into one of three categories, all of which orient the hydrophobic moment of the amphipathic α-helices of the carboxy-terminal lipid-binding domain toward the hydrophobic hydrocarbon chains of the lipid bilayer that form the core of the HDL particle. Picket fence models of apo A-I in discoidal HDL particles are arranged with the long axes of the amphipathic α-helical repeats perpendicular to the plane of the lipid bilayer. In these models, proline residues function as helix breakers, introducing turns into the secondary structure of apo A-I, and connecting the helical repeats (*8*−*11*). In the molecular belt and hairpin models, however, the long axes of the helical repeats are instead oriented parallel to the plane of the lipid bilayer (*11*−*16*).

Previously published models based upon both the picket fence (*17*) and the molecular belt (*18*) have been presented in an attempt to explain the observed behavior of a naturally occurring mutant of apo A-I, apo A-I_{Milano}, in which Arg-173 has been mutated to a cysteine (*19*). A molecular belt model has also been proposed by Klon et al. for a similar naturally occurring Arg → Cys mutation, apo A-I_{Paris}, which occurs at residue 151 (*20*). Structurally, both apo A-I_{Milano} and apo A-I_{Paris} are capable of forming both disulfide-linked homodimers and heterodimers with apo A-II (*19*, *20*). Disulfide-linked homodimers of apo A-I_{Milano} are capable of forming discoidal rHDL particles with POPC. These particles have similar diameters when compared to rHDL particles containing wild-type apo A-I (*21*, *22*). Reconstituted HDL particles made with either apo A-I_{Milano} or apo A-I_{Paris} homodimers have been shown to clear DMPC emulsions and promote cholesterol efflux activity (*21*−*23*), as well as activate LCAT activity, although at a reduced rate compared to that of rHDL particles containing wild-type apo A-I (*22*, *24*).

This review will evaluate the previously proposed models for the binding of apo A-I to discoidal HDL particles in light of the recent fluorescence resonance energy transfer (FRET) and proteolysis data presented by several groups (*25*−*27*). In addition to the all-atom models of the picket fence (*10*) and molecular belt (*12*, *18*) conformations of apo A-I cited earlier, new all-atom models for the apo A-I hairpin first proposed by Rogers et al. (*14*, *15*) will be presented and evaluated in light of the experimental data. Molecular belt and hairpin models describing HDL particles with different diameters will also be discussed. Many of these issues have also been discussed in the excellent review by Brouillette et al. (*11*).

MATERIALS AND METHODS

The molecular belt model (*12*) was used as a starting point for construction of the belt models. Molecular belt models of apo A-I representing the protein bound to HDL particles with diameters of differing sizes (110 and 115 Å) were generated from the initial 105 Å belt model by scaling the radial distribution of all atoms. This method disrupted the ideal bond lengths, so the final models were subjected to 3000 steps of conjugate gradient energy minimization in XPLOR (*28*) using the CHARMM22 force field (*29*). The 11-mer segments were then modeled on an 11-residue α-helical sequence of polyalanine having the same pitch and curvature as the remainder of the belt into which they were incorporated.

The helical hairpin model for apo A-I_{Milano} was constructed from the previously published molecular belt model for apo A-I_{Milano} (*18*) by altering the connectivity of the two monomers near residue Arg-173 using the program O (*30*). The main chain was broken at Arg-173 in both monomers, and rejoined to residue Leu-174 on the opposite monomer. A disulfide bond was added between the two cysteine residues, and the resulting structure was energy minimized in XPLOR as described above.

Construction of the 150 Å diameter disks proceeds in a fashion using all of the techniques described above. For the model with a single helical hairpin, the molecular belt model was expanded to have a radius of curvature equal to 150 Å. Two of these monomers were then docked together in an antiparallel orientation with a helix−helix registration corresponding to the LL5/5 registration of the molecular belt model. These two antiparallel belts covered two-thirds of the circumference needed for a 150 Å diameter HDL particle. The remaining one-third of the circumference was constructed by creating a hairpin from these antiparallel belts that doubled back on itself at residue Gly-129. This hairpin was then docked into the remaining one-third gap in the circumference so that its helical repeat 10 interacted with the helical repeat 10 from one of the belt monomers in a manner identical to that of the molecular belt model. The final structure was then energy minimized as described above. The 150 Å disks that contained three helical hairpins were generated by taking three helical hairpins generated as described and docking them so that each of them covered one-third of the circumference of the 150 Å diameter disk.

The four-helix bundle monomer was constructed from the crystal structure of apo Δ(1−43) A-I (*13*) in the following manner. The coordinates for residues 44−67 of monomer D, 68−129 of monomer A, 130−192 of monomer B, and 193−243 of monomer C were extracted from the crystal structure to form a new model. The breaks in the main chain between residues 67 and 68, 129 and 130, and 192 and 193 were closed by the addition of bonds between those residue pairs, and the resulting structure was energy minimized.

COMPETING MODELS FOR HDL PARTICLES

Picket Fence Models. Picket fence models for the binding of the carboxy-terminal domain of apo A-I to discoidal HDL particles are based upon the similarity of this region's secondary structural elements to transmembrane proteins. Because α-helices have a rise per residue of 1.5 Å, ∼20 residues are required to span the thickness of a lipid bilayer for transmembrane helices in membrane proteins. Given that the carboxy-terminal domain of apo A-I contains eight 22-mer amphipathic α-helical repeats based upon secondary structure prediction (*7*), initial models of apo A-I bound to discoidal HDL particles were constructed with the logical

assumption that the long axes of these helical repeats were perpendicular to the plane of the lipid bilayer (*8*−*10*). The picket fence model also has another advantage, in that it suggests a plausible structural role for the presence of proline residues. The eight 22-mer and two 11-mer amphipathic α-helical repeats in the lipid-binding domain are punctuated at regular intervals by proline residues at the first position in the helical repeat (*31*). In the picket fence model, these proline residues are responsible for the introduction of β-turns that connect consecutive helical repeats in an antiparallel orientation. The idea that these amphipathic α-helical repeats interact with each other in an antiparallel fashion was supported by a combination of experimental and theoretical work by a number of laboratories. Modeling studies indicated that this orientation for the helical repeats of apo A-I was energetically favorable (*32*, *33*), and molecular dynamics simulations of reconstituted HDL (rHDL) particles containing 18-residue consensus peptides suggested that these model systems would be stable in solution out to a time scale of at least 700 ps (*34*). Recent extensions of these simulations show the stability of these model rHDL particles beyond 5 ns (C. J. Sheldahl and S. C. Harvey, unpublished results).

The picket fence model also provides an explanation for the experimental observation that apo A-I spontaneously forms discretely sized discoidal HDL particles when mixed with palmitoyloleoylphosphatidylcholine (POPC) or dimyristoylphosphatidylcholine (DMPC) (*35*, *36*). The picket fence conformation of apo A-I would be able to accommodate a change in particle diameter by removal of amphipathic α-helical repeats from the lipid phase (*35*, *36*). Such removal of the helical repeats from the hydrophobic surface would likely occur two repeats at a time because of the antiparallel orientation of adjacent repeats when bound to lipid. Via removal of two repeats at a time, the adjacent helices could interact with one another to bury their hydrophobic surfaces. Thus, the picket fence model could easily facilitate such structural rearrangements by allowing pairs of helical repeats to swing away from the disk in a hingelike fashion. If a 15 Å separation is assumed, the removal of two helices would therefore reduce the circumference of the rHDL particle by 30 Å, thereby reducing the diameter of the rHDL particle by ∼10 Å (*35*, *36*).

To date, the atomic coordinates for only one published structure for the picket fence model of apo A-I have been made available. Phillips and co-workers have constructed an all-atom model of a discoidal HDL particle with a diameter of 96 Å containing two monomers of apo A-I and 160 molecules of POPC (*10*). In this model, eight 22-mer helical repeats were used to span the circumference of the disk and a smaller amphipathic α-helix that was too small to span the thickness of the bilayer was placed parallel to the plane of the lipid bilayer. This model presented two different arrangements for the apo A-I monomers around the edge of the disk. The two monomers could interact in a head-to-head orientation, placing helix 1 from one molecule and helix 1 from the other adjacent to one another in an antiparallel fashion. Alternatively, in the head-to-tail orientation, helix 1 from one monomer would be antiparallel and adjacent to helix 8 of the other monomer. These two alternate conformations were presented because the experimental evidence available at the time was unable to differentiate between the two conformations. Furthermore, if we assume that the picket fence model is correct, there is no plausible reason for the preference of one orientation over the other, and therefore, both might coexist simultaneously in rHDL particles.

A critical problem with the published picket fence models is that they depend on a separation of 15 Å between the centers of adjacent helices to cover the circumference. Although the presumption of a 15 Å interhelical distance would allow for the discrete particle size heterogeneity observed in rHDL particles, a more realistic value for interhelical distances based upon protein structures determined through X-ray crystallography is closer to 10 Å. In particular, the antiparallel α-helices in the crystal structure of the 200 carboxy-terminal residues of apo A-I are packed with a center-to-center distance of 10 Å (*14*). Furthermore, a 15 Å interhelical separation leaves much of the hydrophobic surface area of the lipid hydrocarbon chains exposed to solvent.

A small discoidal rHDL particle with a total diameter of 105 Å would have an interior diameter of ∼85 Å if the protein is omitted. If a thickness of 30 Å is assumed for the lipid bilayer, combined with the 5 Å of hydrophobic surface not covered between adjacent helical repeats in the picket fence model, 150 $Å^2$ of lipid is exposed to solvent. If we use the value calculated for the hydrophobic effect by Sharp et al. of 47 cal mol^{-1} $Å^{-2}$ (*37*), the resulting free energy of the system is increased by ∼7 kcal/mol per gap between helical repeats. With eight gaps per apo A-I monomer, or 16 gaps per HDL particle, the total increase in energy of the system is ∼112 kcal/mol. It could be argued, however, that the assumptions made to arrive at this value are too conservative. In our molecular dynamics simulations on model rHDL particles, we observe an interhelical distance of ∼12.5 Å, and the lipid headgroups are able to curve over the sides of the disk, reducing the hydrophobic thickness to ∼25 Å (A. E. Klon et al., manuscript in preparation). Applying these more conservative estimates for exposed hydrophobic surface area to the picket fence model, one arrives at a value of 62.5 $Å^2$ for the exposed hydrophobic surface area. If we again use the above value from Honig et al. for the hydrophobic effect, we obtain a penalty of ∼3 kcal/mol per gap, for a total energetic cost of 48 kcal/mol. Even using the far more conservative estimate for the magnitude of the hydrophobic effect of 24 cal mol^{-1} $Å^{-2}$ (*38*), we obtain a value of ∼1.5 kcal/mol per gap, or 24 kcal/mol for a single HDL particle. Because the stabilization energy of HDL particles is ∼2−6 kcal/mol (*39*−*42*), even the most permissive parameters predict that an unacceptable amount of hydrophobic surface area is exposed to solvent in the picket fence model.

Models with helical repeats that have a 10 Å interhelical distance would require more helical repeats to surround the circumference of the HDL particle. This would require an additional monomer of apo A-I to bind to the rHDL particle. Since the stoichiometry of rHDL particles is well-established (*43*), such a model would disagree with current experimental data. In addition, the model for discrete particle sizes brought about via the removal of the amphipathic helices from the particle would no longer hold. Removing two helical repeats from the rHDL particle would reduce the circumference by only 20 Å, with a corresponding decrease of ∼6.7 Å in the

diameter rather than ~10 Å as observed experimentally (*35*, *36*).

A picket fence model of apo A-I_{Milano} has also been presented (*17*). In this model of a disulfide-linked homodimer of apo A-I_{Milano}, the terminal 70 residues from Cys-173 to Glu-243 do not associate with the lipid, but rather "loop out of the HDL surface" (*17*). This model has been used to invoke the experimentally observed restricted particle size heterogeneity of rHDL particles containing disulfide-linked homodimers of apo A-I_{Milano} (*21*). This model shares a number of deficiencies common to the picket fence models discussed previously. In particular, it relies on the requirement that adjacent amphipathic α-helical repeats have an interhelical distance of 15 Å. In addition, helical repeats 8−10 in this model do not associate with the lipid in rHDL particles. This is in contrast to experimental data indicating that helical repeats 1 and 10 have the highest lipid affinity of any of the amphipathic repeats in the carboxy-terminal domain of apo A-I (*44*). The picket fence model of apo A-I_{Milano} bound to discoidal rHDL particles does not agree with experimental data for the binding of amphipathic helices to lipid or the helix−helix distances observed in known protein structures.

Molecular Belt Models. Belt models for the 200-residue carboxy-terminal lipid-binding domain of apo A-I in discoidal rHDL particles are oriented with the long axes of the helical repeats parallel to the plane of the lipid bilayer (*11*−*15*). The resulting structure for the apo A-I monomer resembles a torus bound to the circumference of the disk, with the hydrophobic faces of the amphipathic helical repeats oriented toward the interior of the disk. Such a curvature of amphipathic repeats toward the hydrophobic environment is observed in high-resolution crystal structures of large globular proteins (*45*, *46*). It has been argued that the backbone carbonyl atoms that form hydrogen bonds to side chain atoms and water molecules cause the helical tilt angle to become more pronounced, decreasing the length of backbone hydrogen bonds in the hydrophobic environment while increasing the length of backbone hydrogen bonds in the hydrophilic environment (*45*). For the smaller discoidal HDL particles with diameters of ~100 Å, 200 residues is enough to cover the circumference if the ideal rise per residue of 1.5 Å for an α-helix is assumed. The stoichiometry of rHDL particles of this size has been well established to be two monomers of apo A-I per particle (*43*). Consistent with these data, our molecular belt model has been constructed with two monomers of apo A-I for a discoidal HDL particle 105 Å in diameter (*13*, *18*).

The molecular belt model can also provide an explanation for the experimentally observed discretely sized rHDL particles. An analysis of the entire 243-residue length of apo A-I by the LOCATE program (*47*) suggests that there are as many as three additional 11-mer amphipathic α-helical repeats in the amino-terminal 43-residue domain of apo A-I (*7*). In the belt model, the carboxy-terminal 200 residues would be enough to cover the circumference of a 105 Å discoidal rHDL particle, assuming no gap between the amino- and carboxy-terminal ends of the protein. The addition of an 11-mer amphipathic helical repeat spanning residues 33−43 of the amino-terminal domain could accommodate a discoidal rHDL particle with a diameter of 110 Å (Figure 1). Similarly, the addition of another 11-mer helical repeat from the amino-terminal domain of apo A-I would increase the diameter of the resulting rHDL particle to 115 Å (Figure 1).

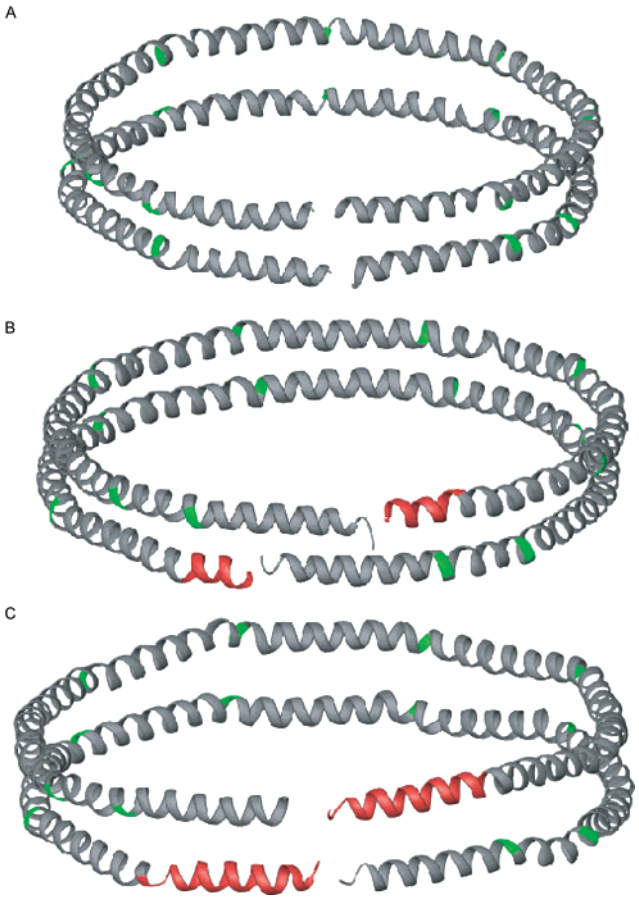

FIGURE 1: Molecular belt models for discoidal rHDL particles with three different diameters. (A) The 200-residue lipid-binding domain of apo A-I forms a disk with a diameter of 105 Å. (B) The addition of an 11-mer repeat (red) from the N-terminal 43-residue domain increases the particle size to 110 Å. (C) The addition of two 11-mer repeats from the N-terminal domain (red) increases the particle size to 115 Å. Prolines that punctuate the amphipathic repeats are shown in green. This figure was generated with Ribbons (*49*).

The belt model could further accommodate the smaller diameter discoidal HDL particles by the removal of one or more helical repeats from each monomer in a manner similar to one proposed previously for the picket fence model. The molecular belt model published by Segrest et al. predicts that the helix 5−helix 5 interaction would be the weakest, based upon the consideration of interhelical salt bridges (*12*, *13*). Indeed, a 1 ns molecular dynamics simulation carried out recently by this laboratory on a discoidal HDL particle containing 160 molecules of POPC and two monomers of apo A-I shows that the interhelical distance between helix 5 and helix 5 is substantially wider than the interhelical distances for the rest of the repeats (A. E. Klon et al., manuscript in preparation). If the 22 residues of the helical repeat 5 pair were displaced from the outside of the disk so that they no longer interacted with the lipid, this would constitute a loss of another 33 Å from the circumference of the disk. The diameter of the disk is then reduced by ~10 Å, resulting in a diameter of 95 Å for the smaller rHDL particles in the molecular belt model. This model for the removal of one or more amphipathic repeats from the circumference of the rHDL particle has been proposed as a

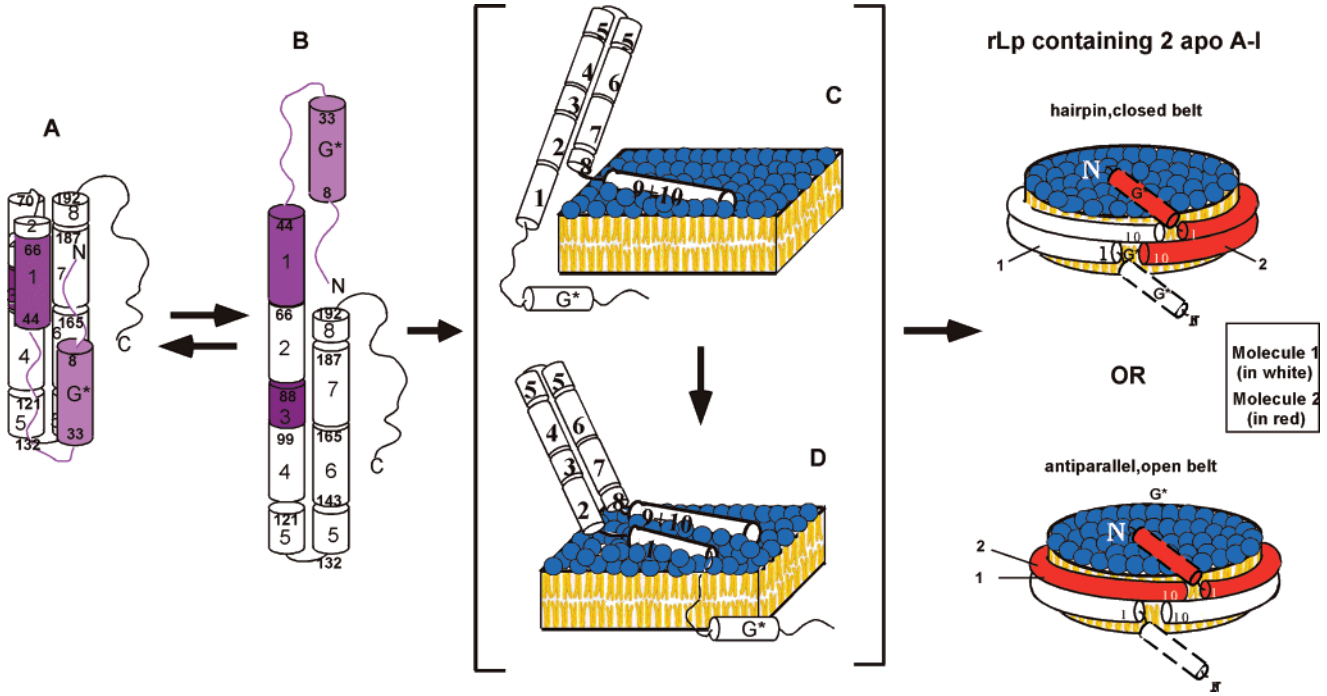

FIGURE 2: Hypothetical structure-based lipid binding mechanism for human apo A-I. (A) Proposed tertiary structural model of lipid-free apo A-I depicting a folded helical bundle. (B) Elongated monomeric helical hairpin derived via analytical ultracentrifugation (*14*). The purple shaded regions represent those deleted in the mutants studied in ref *15*. Helices are numbered according to the repeating sequence homology (*7*, *11*, *50*). (C) Initial lipid-binding step of lipid-free apo A-I mediated through a largely unfolded and uncooperative carboxy-terminal domain. Binding of these residues is associated with an increase in the overall α-helicity of the protein. (D) Later intermediate produced following a conformational switch of residues 1−43 which unmasks a latent lipid-binding domain, most likely represented by the residues of helix 1 (amino acids 44−65). Final products are depicted here as discoidal lipoproteins containing two apo A-I molecules. The perpendicular orientation relative to the acyl chains of the lipids is suggested by the crystal structure of apo Δ(1−43) A-I (*13*) and other biophysical studies (*16*, *25*, *51*, *52*). This figure was adapted from ref *15* and was kindly provided by C. G. Brouillette.

variation of the hinged domain model for changes in rHDL size for the picket fence (*27*) and molecular belt models (L. Li and J. P. Segrest, manuscript in preparation).

In the picket fence model, proline residues introduce turns between helical repeats, but they serve a different function in the molecular belt model. The proline residues in the belt model are hypothesized to introduce regular kinks in the sequence of the lipid-binding domain to properly orient the hydrophobic face of the amphipathic helical repeats for proper lipid binding (*12*, *13*). In the apo A-I crystal structure, the kinks introduced by the proline residues are observed to have a mean kink angle of 40° with a standard deviation of 17° (*13*). The molecular belt model places these proline residues on the outside of the helical torus to force the helical repeats into a circular, planar structure (*12*). This is observed in the crystal structure (*13*) and is consistent with other protein structures in which the proline residues are on the hydrophilic face of the helix, causing the helix to curve toward the hydrophobic face (*46*, *48*).

We have previously proposed a molecular belt model for apo A-I_{Milano} (*18*). This model is based upon experimentally observed data for rHDL particle sizes containing a single disulfide-linked homodimer of apo A-I_{Milano} and DMPC. The previously published molecular belt models offer an attractive explanation for the presence of an intermolecular disulfide bond, because the monomers only need to rotate relative to one another until Cys-173 on each chain is juxtaposed with its equivalent on the opposite chain. The molecular belt model for apo A-I_{Milano} is thus structurally similar to rHDL particles containing wild-type apo A-I. This structural similarity explains the experimental observations that particles containing apo A-I_{Milano} are capable of LCAT activation, clearing DMPC emulsions, and promoting cholesterol efflux (*21*, *24*).

Helical Hairpin Models. Hairpin models for the binding of apo A-I to discoidal HDL particles provide three advantages: an attractive explanation for the mechanism of lipid binding, preservation of the interhelical interactions observed in the crystal structure of Borhani et al. (*13*), and a model for discoidal rHDL particles containing three monomers of apo A-I.

Rogers et al. (*14*, *15*) have argued that the helical hairpin offers the simplest explanation for the transition from lipid-free to lipid-bound apo A-I. The crystal structure of lipid-free apo A-I revealed a tetramer in which the helical repeats of apo A-I formed a four-helix bundle (*13*). Rogers et al. proposed that in solution apo A-I is present as a four-helix bundle that is in equilibrium with a helical hairpin conformation that binds to lipid to form discoidal HDL particles (Figure 2). They proposed that the four-helix bundle monomer could be generated from the X-ray crystal structure of apo Δ(1−43) A-I (*13*) by changing the connectivity of the amino acid residues (Figures 3 and 4). Where two residues on antiparallel chains are juxtaposed in the crystal structure, the main chain was made to double back on itself. The coordinates for the bulk of the atoms were unchanged, with the exception of those residues at the ends of the helices that are now participating in turns. The resulting four-helix bundle monomer shown in Figure 4 contains helices from all four monomers in the apo Δ(1−43) A-I crystal structure.

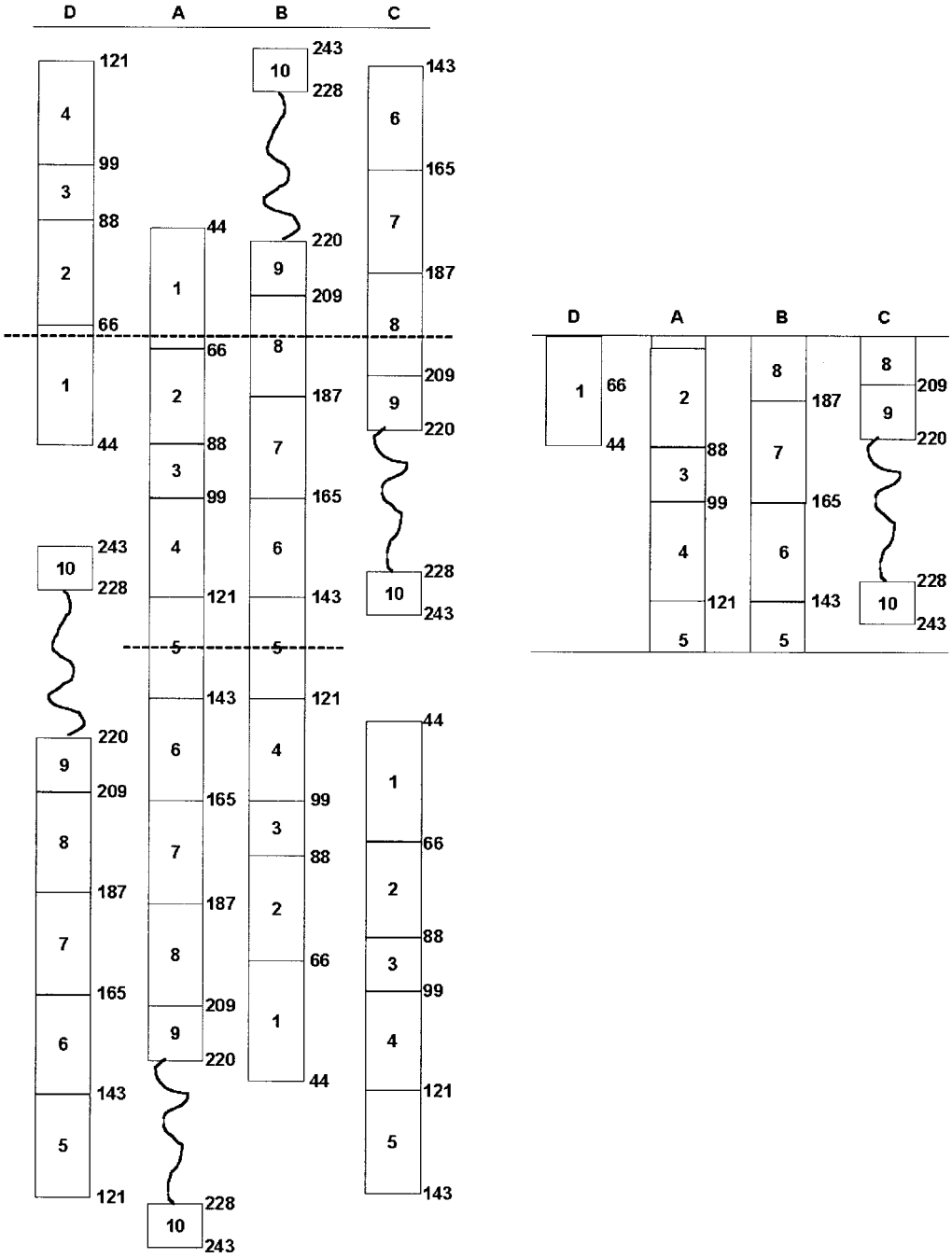

FIGURE 3: Schematic diagram of how a four-helix bundle monomer (right) can be extracted from the crystal structure of apo Δ(1−43) A-I reported by Borhani et al. (*13*) (left). Four such four-helix bundles are found in the crystal structure, each one containing the complete 200-residue carboxy-terminal domain of apo A-I (residues 44−243). This figure is courtesy of C. G. Brouillette.

Both the helical hairpin and molecular belt models assume that the driving force behind lipid binding is the hydrophobic effect, and rHDL particles with diameters of 105, 110, and 115 Å can be formed with both models using the same experimentally determined stoichiometry of apo A-I to POPC. In these models, two monomers of apo A-I wrap around the circumference of the disk with their helical axes parallel to the lipid bilayer. In the helical hairpin model, the monomers fold back on themselves in the middle of helix 5, causing helical repeats 1−4 to be oriented in an antiparallel fashion with repeats 6−10 of the same monomer rather than with the other monomer as in the belt model. In the belt model, Gly-129 from one monomer is juxtaposed with Gly-129 from the other monomer; the helical hairpin model doubles back on itself with a turn at Gly-129. It is interesting to note that helix 5 is predicted by the belt model to have the poorest interhelical interactions. Because the helix−helix registrations are predicted to be identical in the two models, the interhelical salt bridges are also predicted to be identical, with the difference being that these salt bridges in the helical hairpin would be intramolecular, as opposed to the intermolecular salt bridges proposed in the molecular belt model. In the helical hairpin, the hydrophobic face of the amphipathic α-helical repeats curves toward the lipid for the same reasons previously argued in the molecular belt model (*12*, *45*). Proline punctuation serves the same function in the helical hairpin model as it does in the molecular belt model, introducing kinks at regular intervals along the length of the

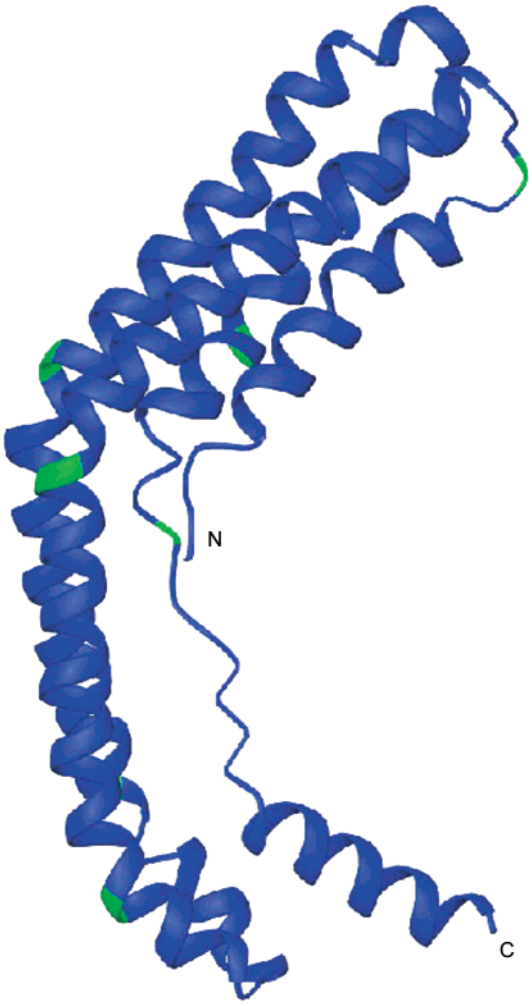

FIGURE 4: Ribbons (*49*) model of the four-helix bundle proposed by Rogers et al. (*15*). The model was generated by cutting a piece out of the apo Δ(1−43) A-I tetramer from the crystal structure reported by Borhani et al. (*13*) as shown in Figure 3. The helices from the four monomers were then connected.

helices to properly orient the hydrophobic face of the helices for lipid binding (*12*).

On the basis of the helical hairpin, two different models for 150 Å diameter discoidal HDL particles with three monomers of apo A-I per disk can be constructed (Figure 5). In the first model (Figure 5A), two monomers of apo A-I interact with one another in an antiparallel fashion as in the molecular belt model, but with an increased radius of curvature, allowing them to cover two-thirds of the circumference of the disk. The final one-third of the circumference of the disk is covered by a helical hairpin as described above, but with a corresponding increase in the radius of curvature. The second model (Figure 5B) consists of three helical hairpins, each spanning one-third of the circumference of the HDL particle. In both of these models, the interhelical interactions, intermolecular as well as intramolecular, are identical to those predicted in the molecular belt model. It is important to note that at least one helical hairpin is required for any disk containing three apo A-I molecules.

Helical hairpin models can also be constructed for the apo A-I_{Milano} and apo A-I_{Paris} mutations. In the molecular belt models for these mutations, the monomers were rotated relative to one another until residue Cys-173 (apo A-I_{Milano}) or Cys-151 (apo A-I_{Paris}) was juxtaposed, thus bringing the

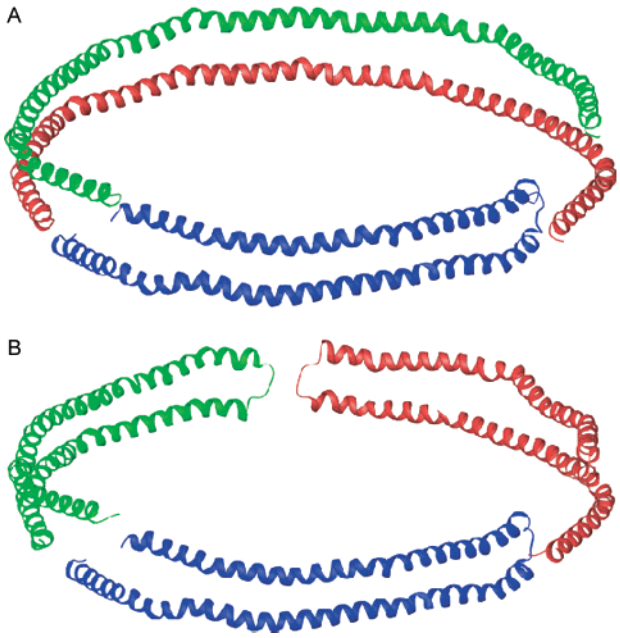

FIGURE 5: Two different models for the discoidal 150 Å rHDL particle. (A) Two monomers of apo A-I associate in an antiparallel fashion (red and green), while a third monomer is present as a helical hairpin (red). (B) Three monomers in the helical hairpin conformation forming the same size particle. This figure was generated with Ribbons (*49*).

two cysteine residues close enough to form a disulfide bridge (*18*). To form the disulfide-linked homodimers of apo A-I_{Milano} or apo A-I_{Paris}, the hairpins would have to double back on themselves at residue Cys-173 or Cys-151, respectively. This contrasts with the hairpin model with the same interhelical interactions as in the crystal structure (*13*) and the molecular belt model (*12*), where the turn is centered at Gly-129. The molecular belt model was an attractive explanation for the formation of disulfide-linked homodimers in the mutant HDLs, because the monomers can be rotated such that the γ-sulfur atoms can be brought within covalent bonding distance without either distorting the local helical structure or changing the 10 Å interhelical distance between the two monomers. In the helical hairpin, however, introducing a turn at residue 173 or 151 and positioning the cysteine residues such that their side chains would be able to form a disulfide bond without further distortion of the local secondary structure of apo A-I require a very precise, but feasible, placement of the turn (Figure 6). Alternatively, the hairpins could double back on themselves at approximately residue 28 in the middle of helical repeat 2 (apo A-I_{Milano}) or at approximately residue 6 in the middle of helical repeat 1 (apo A-I_{Paris}). It seems unlikely that interhelical interactions would be able to stabilize such short helical hairpin structures.

In contrast to the hairpin model with the interhelical interactions discussed above, the intramolecular antiparallel arrangement of the α-helices in the Milano hairpin model is no longer continuous due to the introduction of a turn around residue 173. This leaves helical repeats 1−3 to form intermolecular interactions with helical repeats 1−3 of the opposite monomer (Figure 6), suggesting that the mutant apo A-I monomers first bind to discoidal HDL particles in the helical hairpin conformation proposed by Rogers et al. (*15*), helix−helix registration. This would require the intra-

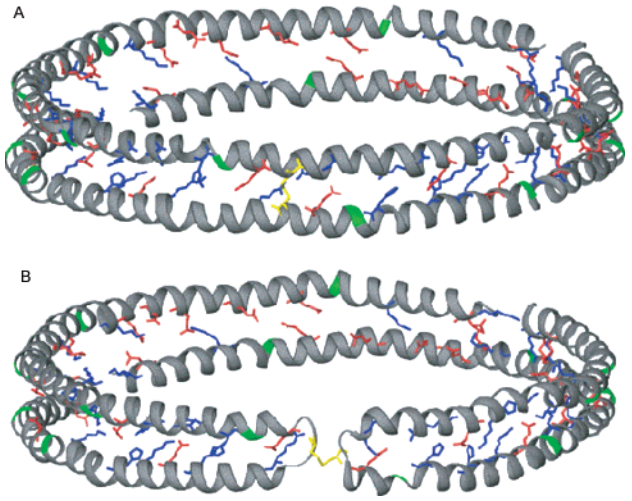

FIGURE 6: Two different models for discoidal rHDL particles containing two disulfide-linked monomers of apo A-I$_{Milano}$. Panel A is a belt model, while panel B contains two helical hairpins. The hairpins differ from those in Figure 2 in the location of the reverse turn. This figure was generated with Ribbons (*49*).

molecular helical interactions to break apart as the loop walks through the sequence and then form new intramolecular or intermolecular helical interactions once the loop has passed through the sequence until the cysteines are brought into sufficient proximity in the loop region to form a disulfide bond. This mechanism would further require that the loop walk along the sequence of the protein in the same direction and at the same rate in both monomers. If this mechanism is correct, it suggests that for the wild-type apo A-I, alternative helical registrations are possible.

EXPERIMENTAL EVALUATION OF COMPETING MODELS

FRET Studies. In principle, distance measurements from fluorescence resonance energy transfer (FRET) experiments should be able to distinguish between the various models for apo A-I bound to discoidal HDL particles. Here we show that recent FRET measurements (*25*, *26*) appear to rule out the picket fence model of apo A-I but are unable to distinguish between the molecular belt and helical hairpin models. These experiments in both laboratories were carried out on rHDL particles containing two monomers of apo A-I and either DMPC or POPC. The distances measured from the FRET data reported by these two groups are presented in Table 1, along with the predicted distances for each of the models. In addition to the experimentally determined distances, Tricerri et al. also reported corrected FRET distances to compensate for the possibility that two donor fluorescence probes would be present in 25% of the rHDL particles, assuming a random distribution of apo A-I monomers.

Li et al. (*25*) reported a FRET distance of 6 Å between donor−acceptor pairs at position 132 of apo A-I. This strongly supports the molecular belt model, which has a predicted distance of 16 Å between the α-carbons of these two residues, compared to distances of 31 Å for the head-to-head helical hairpin and distances of ∼100 Å for the tail-to-tail helical hairpin and the picket fence models. Even though a distance of 16 Å should result in greatly increased transfer efficiency, approaching 100%, the observed transfer efficiency was only 45%. The authors attributed the differences in expected transfer efficiency to an uneven distribution of apo A-I monomers with donor−acceptor probes in the same rHDL particle. In contrast, Tricerri et al. (*26*) also reported the FRET distances that included the correction factor described above. They have argued that a transfer efficiency of 40% for the Cys-132 mutant observed by Li et al. actually correlates well with their observed transfer efficiency for the Cys-124 mutant, which has a value of 45%. Using the Tricerri model for FRET distances, a distance of 45−50 Å is obtained from the Cys-124 mutant. On the basis of these data, Tricerri et al. argued that neither the picket fence nor the belt model was supported by the data, but rather, the FRET distances agreed with the presence of two hairpins in a rHDL particle, distributed equally between the head-to-head and head-to-tail conformations. The fact that two different laboratories have carried out essentially the same experiment and yet obtained different values indicates that the results of FRET measurements should be viewed with caution.

Table 1: Comparison of Calculated Distances between Fluorescence Donors and Acceptors with Previously Published Data Experimentally Determined from FRET Measurements Reported by Tricerri et al. (1) and Li et al. (2)[a]

donor−acceptor positions	calculated distance (Å)				measured distance (Å)	
	belt model	picket fence	hairpin, head to head	hairpin, head to tail	exptl	corrected
9−9	–	–	–	–	63[1]	78[1]
124−124	23	83	29	93	47[1]	76[1]
132−132	16	104	31	97	6[2]	–
232−232	12	74	10	100	53[1]	77[1]
9−232	–	–	–	–	56[1]	81[1]

[a] Corrected distances were calculated by Li et al. from corrected fluorescence lifetimes to compensate for the presence of two donor molecules in a single rHDL particle.

A possible solution, however, is that the monomers may rotate relative to one another about the circumference of the rHDL particle, resulting in different helix−helix registrations. It was hypothesized on the basis of a heuristic salt bridge scoring function that, although the LL5/5 rotamer was the preferred conformation, different helix−helix registrations could result in favorable rotamers with slightly higher salt-bridging scores (*12*). Indeed, recent cross-linking studies have suggested that rHDL particles may favor the LL5/6 rotamer, while the previously published LL5/5 rotamer, and to a lesser extent the LL5/4 rotamer, are also highly favored registrations (L. Li and J. P. Segrest, manuscript submitted for publication). The observed transfer efficiencies could therefore be explained by either the molecular belt or the helical hairpin model. In the helical hairpin model, the transfer efficiencies would be a result of a mixture of rHDL particles evenly divided between hairpins interacting with each other by a head-to-head orientation or via a head-to-tail orientation, as proposed by Tricerri et al. Since transfer efficiencies are additive, the rotation of one monomer with respect to the other in the belt model would give rise to an ensemble of rHDL particles with different helix−helix registrations and could result in similar transfer efficiencies.

Proteolysis Data. Recently, proteolysis experiments were carried out on small (78 Å) discoidal rHDL particles containing POPC and either wild-type apo A-I or disulfide-

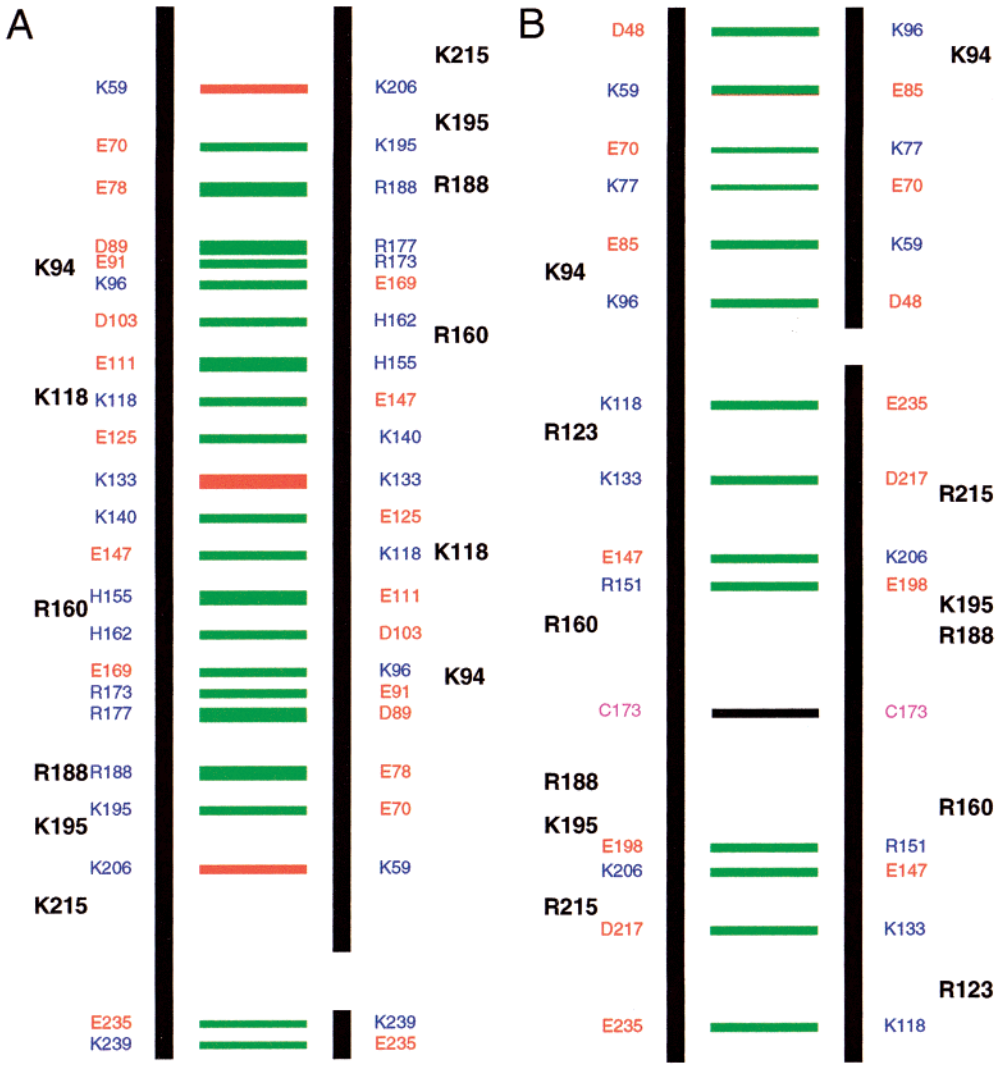

FIGURE 7: Location of salt bridges predicted in the wild-type (A) and Milano (B) rotamers. Acidic residues are red, and basic residues are blue. Salt bridges are green, while charge appositions between like charges are red. The residues marking the location of trypsin cleavage sites are black. The locations of the R173C mutations for apo A-I_{Milano} are violet, and the corresponding disulfide bond between them is black.

linked homodimers of apo A-I_{Milano} (*27*). Trypsin cleavage sites for small discoidal rHDL particles containing two monomers of wild-type apo A-I occurred at residues Lys-94, Lys-118, Arg-160, Arg-188, Lys-195, and Arg-215, with 50% of the protein being cleaved after incubation for 6 h. In contrast, the smaller discoidal rHDL particles containing a single disulfide-linked homodimer of apo A-I_{Milano} were found to be 50% cleaved after incubation for only 10 min with trypsin. The trypsin cleavage sites for apo A-I_{Milano} were similar to those in the wild type, with cleavage sites located at residues Lys-94, Lys-123, Arg-160, Arg-188, Lys-195, and Arg-215.

Figure 7 shows the location of the predicted interhelical salt bridges for the wild-type apo A-I and apo A-I_{Milano} registrations for the molecular belt models (*12*, *18*). Also shown are the locations of the trypsin cleavage sites reported by Calabresi et al. (*27*). In rHDL particles containing wild-type apo A-I, proteolysis was immediately observed after residues Arg-215, Lys-195, and Lys-118, followed by cleavage at Arg-188, Arg-160, and Lys-94. Proteolysis in rHDL particles containing disulfide-linked homodimers of apo A-I_{Milano} first occurs after residues Arg-123, Arg-160, Arg-188, Lys-195, and Arg-215, followed by cleavage after Lys-94. Cleavage was also observed to occur more quickly in the rHDL particles containing apo A-I_{Milano}, with 50% cleavage observed after 10 min, as opposed to 6 h for 50% cleavage in rHDL particles containing wild-type apo A-I. The location of the proteolysis sites and the rates of proteolysis in the two forms of apo A-I are quite striking and illustrate a clear structural difference between the LL5/5 and Milano molecular belt models. In the LL5/5 belt model, three of the residues cleaved are participating in interhelical salt bridges: Lys-118, Arg-188, and Lys-195. Of the remaining residues that were cleaved, two of them (Lys-94 and Arg-160) are flanked by side chains which are participating in interhelical salt bridges. The remaining cleavage site at Lys-215 is some distance away from any interhelical salt bridges. In the case of the apo A-I_{Milano} belt model, however, three of the cleavage sites cleaved first (Arg-160, Arg-188, and Lys-195) bracket a region ~22 residues in either direction along the sequence from the disulfide bond at residue Cys-173. It is also interesting to note that none of the residues cleaved by trypsin in the rHDL particles containing apo A-I_{Milano} are predicted by the belt model to

be participating in interhelical salt bridges, and that there are predicted to be fewer interhelical salt bridges in the apo A-I$_{Milano}$ model than in the wild-type apo A-I belt model. There is a strong inverse correlation between the strength of interhelical interactions predicted in the belt model (*12*) and the rate of proteolysis (*27*). The data presented by Calabresi et al. therefore support one of the central hypotheses of the molecular belt model, that is, that while the hydrophobic effect provides the driving force for the structure of apo A-I when it is bound to lipid in rHDL particles, the interhelical salt bridges are vital to stabilizing interhelical interactions between the monomers (*12*).

CONCLUSIONS

We have presented several new models for apo A-I bound to rHDL particles with different diameters in addition to the previously reported 105 Å diameter molecular belt model (*12*). All-atom molecular belt models now exist for rHDL particles with diameters of 110 and 115 Å. Two separate models for an rHDL particle with a diameter of 150 Å have also been presented, one which contains two monomers of apo A-I in a belt conformation and one monomer of apo A-I in a helical hairpin conformation, and a second model which contains three apo A-I monomers, all in helical hairpin conformations. We have also evaluated the previously published all-atom models for the picket fence and molecular belt along with these new models in light of recent experimental evidence.

The advantages of the picket fence model are that it can explain the presence of proline residues in the sequence of the lipid-binding domain at regular intervals and that it also suggests a mechanism for transitions between discoidal rHDL particles with discrete diameters. However, the picket fence model is incompatible with theoretical arguments and experimental data. The 15 Å distance between the centers of adjacent helices in the model is larger than that observed in protein crystal structures, particularly the lipid-free crystal structure of the Δ43 mutant (*13*). This leaves a large amount of hydrophobic surface area on the lipid hydrocarbon chains exposed to solvent. In addition to the X-ray crystal structure, Fourier transform infrared (FTIR) spectroscopy and FRET measurements both indicate that the axes of the helical repeats lie perpendicular to the normal of the lipid bilayer (*16*, *25*, *26*), which is inconsistent with picket fence models.

The molecular belt model for apo A-I bound to discoidal rHDL particles is able to explain a number of experimental observations. Most directly, the X-ray crystal structure of the Δ43 mutant of apo A-I (*13*) and recent FTIR data of rHDL particles containing full-length apo A-I (*16*) strongly suggest an arrangement in which the long axes of the amphipathic α-helices are perpendicular to the normal of the lipid bilayer. The belt models presented in this paper also explain the presence of rHDL particles with discrete diameters. The molecular belt model can also be used to explain the observation that rHDL particles with wild-type apo A-I and apo A-I$_{Milano}$ have similar diameters (*18*). There is one confounding piece of experimental evidence, however, the observation that rHDL particles made with DMPC appear to have larger diameters than rHDL particles made with POPC. The previously published belt model for apo A-I$_{Milano}$ assumes rHDL particles with DMPC that match the diameters of small discoidal rHDL particles with wild-type apo A-I. As pointed out by Tricerri et al., the apo A-I$_{Milano}$ belt model does not explain the presence of rHDL particles with diameters of 78 Å made with POPC. To our knowledge, there has been no direct comparison of rHDL diameters for wild-type and mutant apo A-I constructed with POPC and DMPC. Neither the picket fence, helical hairpin, nor belt model explains the apparent reason for structural changes between rHDL particles with different lipid compositions, though it is likely due to both shorter chain length and saturation of the myristoyl chains.

The helical hairpin model for apo A-I in rHDL particles is also able to explain a number of experimental observations, and it holds some advantages over the molecular belt model. The helical hairpin could in principle explain the discrete particle size heterogeneity observed in rHDL particles, but the pathway for the transition between these rHDL particles with different diameters is less clear. One of the advantages of the helical hairpin is that it does provide a model for 150 Å discoidal rHDL particles constructed using DMPC, because we can easily accommodate an uneven number of apo A-I hairpin monomers around such a disk. We have presented two separate models for the 150 Å discoidal particles, and in both of them, the helical hairpin plays a key structural role. If these models are correct, it suggests that the helical hairpin could be present in smaller rHDL particles, perhaps in conjunction with the molecular belt conformations.

The recent FRET data (*25*, *26*) appear to be incompatible with the picket fence model for HDL binding. The data do not appear to distinguish between the molecular belt model and the helical hairpin model for two reasons. The two groups examined what was essentially the same apo A-I mutant with fluorescence probes, Q132C and A124C. Despite the proximity of these two residues to one another, the two groups reached different conclusions regarding the lipid-bound structure of apo A-I. While Li et al. suggested that the transfer efficiency measured for the Q132C mutant was consistent with the molecular belt, Tricerri et al. argued that the transfer efficiency observed for the A124C mutant supported the helical hairpin model. What neither group considered was that, while the molecular belt model has a distinct preference for a specific helix−helix registration, there might be other favorable rotamers. The belt model predicts that these rotamers would be less favorable than the one observed in the crystal structure of Δ43 apo A-I, but some fraction of these less favorable apo A-I rotamers would nevertheless be present (*12*).

ACKNOWLEDGMENT

Christie Brouillette first observed that the helical hairpin model for the apo A-I monomer is clearly implied by the crystal structure of apo Δ(1−43) A-I. We thank her for many exciting discussions, for providing Figures 2 and 3, and for critically reading the manuscript.

REFERENCES

1. Miller, N. E., Thelle, D. S., Førde, O. H., and Mjøs, O. D. (1977) *Lancet 1*, 965−968.
2. Miller, G. J., and Miller, N. E. (1975) *Lancet 1*, 16−19.

3. Castelli, W. P., Garrison, R. J., Wilson, P. W. F., Abbot, R. D., Kalousdian, S., and Kannel, W. B. (1986) *JAMA, J. Am. Med. Assoc. 256*, 2835−2838.
4. Rothblat, G. H., Mahlberg, F., Johnson, W. J., and Phillips, M. C. (1992) *J. Lipid Res. 33*, 1091−1097.
5. Luo, C., and Li, W. (1986) *Mol. Biol. 187*, 325−340.
6. Segrest, J. P., Jackson, R. L., Morrisett, J. D., and Gotto, A. M., Jr. (1974) *FEBS Lett. 38*, 247−253.
7. Segrest, J. P., Jones, M. K., De Loof, H., Brouillette, C. G., Venkatachalapathi, Y. V., and Anantharamaiah, G. M. (1992) *J. Lipid Res. 33*, 141−166.
8. Tall, A. R., Small, D. M., Deckelbaum, R. J., and Shipley, G. G. (1977) *J. Biol. Chem. 252*, 4701−4711.
9. Nolte, R. T., and Atkinson, D. (1992) *Biophys. J. 63*, 1221−1239.
10. Phillips, J. C., Wriggers, W., Li, Z., Jonas, A., and Schulten, K. (1997) *Biophys. J. 73*, 2337−2346.
11. Brouillette, C. G., Anantharamiah, G. M., Engler, J. A., and Borhani, D. W. (2001) *Biochim. Biophys. Acta 1531*, 4−46.
12. Segrest, J. P., Jones, M. K., Klon, A. E., Sheldahl, C. J., Hellinger, M., De Loof, H., and Harvey, S. C. (1999) *J. Biol. Chem. 274*, 31755−31758.
13. Borhani, D. W., Rogers, D. P., Engler, J. A., and Brouillette, C. G. (1997) *Proc. Natl. Acad. Sci. U.S.A. 94*, 12291−12296.
14. Rogers, D. P., Roberts, L. M., Lebowitz, J., Engler, J. A., and Brouillette, C. G. (1998) *Biochemistry 37*, 945−955.
15. Rogers, D. P., Roberts, L. M., Lebowitz, J., Datta, G., Anantharamaiah, G. M., Engler, J. A., and Brouillette, C. G. (1998) *Biochemistry 37*, 11714−11725.
16. Koppaka, V., Silvestro, L., Engler, J. A., Brouillette, C. G., and Axelsen, P. H. (1999) *J. Biol. Chem. 274*, 14541−14544.
17. Sirtori, C. R., Calabresi, L., and Franceschini, G. (1999) *Atherosclerosis 142*, 29−40.
18. Klon, A. E., Jones, M. K., Segrest, J. P., and Harvey, S. C. (2000) *Biophys. J. 79*, 1679−1685.
19. Weisgraber, K. H., Rall, S. C., Bersot, T. P., Mahley, R. W., Franceschini, G., and Sirtori, C. R. (1983) *J. Biol. Chem. 258*, 2508−2513.
20. Bruckert, E., von Eckardstein, A., Funke, H., Beucler, I., Wiebusch, H., Turpin, G., and Assman, G. (1997) *Atherosclerosis 128*, 121−128.
21. Calabresi, L., Vecchi, G., Frigerio, F., Vavassori, L., Sirtori, C. R., and Franceschini, G. (1997) *Biochemistry 36*, 12428−12433.
22. Daum, U., Langer, C., Duverger, N., Emmanuel, F., Benoit, P., Denefle, P., Chirazi, A., Cullen, P., Pritchard, P. H., Bruckert, E., Assman, G., and von Eckardstein, A. (1999) *J. Mol. Med. 77*, 614−622.
23. Franceschini, G., Calabresi, L., Chiesa, G., Parolini, C., Sirtori, C. R., Canavesi, M., and Bernini, F. (1999) *Arterioscler., Thromb., Vasc. Biol. 19*, 1257−1262.
24. Calabresi, L., Franceschini, G., Burkybile, A., and Jonas, A. (1997) *Biochem. Biophys. Res. Commun. 232*, 345−349.
25. Li, H., Lyles, D. S., Thomas, M. J., Pan, W., and Sorci-Thomas, M. G. (2000) *J. Biol. Chem. 275*, 37048−37054.
26. Tricerri, M. A., Agree, A. K. B., Sanchez, S. A., Bronski, J., and Jonas, A. (2001) *Biochemistry 40*, 5065−5074.
27. Calabresi, L., Tedeschi, G., Treu, C., Ronchi, S., Galbiati, D., Airoldi, S., Sirtori, C. R., Marcel, Y., and Franceschini, G. (2001) *J. Lipid Res. 42*, 935−942.
28. Brünger, A. T. (1992) *XPLOR*, The Howard Hughes Medical Institute and Department of Molecular Biophysics and Biochemistry, Yale University, New Haven, CT.
29. Brooks, B. R., Bruccoleri, R. E., Olafson, B. D., States, D. J., Swaminathan, S., and Karplus, M. (1983) *J. Comput. Chem. 4*, 187−217.
30. Jones, T. A., Zou, J. Y., Cowan, S. W., and Kjelgaard, M. (1991) *Acta Crystallogr. A47*, 110−119.
31. Boguski, M. S., Freeman, M., Elshourbagy, N. A., Taylor, J. M., and Gordon, J. I. (1986) *J. Lipid Res. 27*, 1011−1034.
32. Brasseur, R., De Meutter, J., Vanloo, B., Goormaghtigh, E., Ruysschaert, J. M., and Rosseneu, M. (1990) *Biochim. Biophys. Acta 1043*, 245−252.
33. Brasseur, R., Lins, L., Vanloo, B., Ruysschaert, J. M., and Rosseneu, M. (1992) *Proteins: Struct., Funct., Genet. 13*, 246−257.
34. Sheldahl, C. J., and Harvey, S. C. (1999) *Biophys. J. 76*, 1190−1198.
35. Brouillette, C. G., Jones, J. L., Ng, T. C., Kercret, H., Chung, B. H., and Segrest, J. P. (1984) *Biochemistry 23*, 359−367.
36. Jonas, A., Kezdy, K. E., and Wald, J. H. (1989) *J. Biol. Chem. 264*, 4818−4824.
37. Sharp, K. A., Nicholls, A., Fine, R. F., and Honig, B. (1991) *Science 252*, 106−109.
38. Richards, F. M. (1977) *Annu. Rev. Biophys. Bioeng. 6*, 151−176.
39. Reijngoud, D. J., and Phillips, M. C. (1982) *Biochemistry 21*, 2969−2976.
40. Sparks, D. L., Phillips, M. C., and Lund-Katz, S. (1992) *J. Biol. Chem. 267*, 25830−25838.
41. Davidson, W. S., Hazlett, T., Mantulin, W. W., and Jonas, A. (1996) *Proc. Natl. Acad. Sci. U.S.A. 93*, 13605−13610.
42. Davidson, W. S., Arnvig-McGuire, K., Kennedy, A., Kosman, J., Hazlett, T. L., and Jonas, A. (1999) *Biochemistry 38*, 14387−14395.
43. Jonas, A., Wald, J. H., Toohill, K. L. H., Krul, E. S., and Kézdy, K. E. (1990) *J. Biol. Chem. 265*, 22123−22129.
44. Palgunachari, M. N., Mishra, V. K., Lund-Katz, S., Phillips, M. C., Adeyeye, S. O., Alluri, S., Anantharamaiah, G. M., and Segrest, J. P. (1996) *Arteriocler., Thromb., Vasc. Biol. 16*, 328−338.
45. Blundell, T., Barlow, D., Borkakoti, N., and Thornton, J. (1983) *Nature 306*, 281−283.
46. Barlow, D. J., and Thornton, J. M. (1988) *J. Mol. Biol. 201*, 601−619.
47. Jones, M. K., Anantharamaiah, G. M., and Segrest, J. P. (1992) *J. Lipid Res. 33*, 287−296.
48. MacArthur, M. W., and Thornton, J. M. (1991) *J. Mol. Biol. 218*, 397−412.
49. Carson, M. (1997) *Methods Enzymol. 277*, 493−505.
50. Brouillette, C. G., and Anantharamaiah, G. M. (1995) *Biochim. Biophys. Acta 1256*, 103−129.
51. Maiorano, J. N., and Davidson, W. S. (2000) *J. Biol. Chem. 275*, 17374−17380.
52. Panagotopulos, S. E., Horace, E. M., Maiorano, J. N., and Davidson, W. S. (2001) *J. Biol. Chem. 276*, 42965−42970.

BI020315M